Article

Surface-confined building of Au@Pt-centered and multi-G-quadruplex/hemin wires-surrounded electroactive supernanostructures for ultrasensitive monitoring of morphine

Wei Chen, Lijun Yang, Chao Yan, Bangben Yao, Jian-feng Lu, Jianguo Xu, and Guodong Liu

ACS Sens., **Just Accepted Manuscript** • DOI: 10.1021/acssensors.0c01230 • Publication Date (Web): 07 Jul 2020

Just Accepted

is published by the American Chemical Society. 1155 Sixteenth Street N.W., Washington, DC 20036

Surface-confined building of Au@Pt-centered and multi-G-quadruplex/hemin wires-surrounded electroactive supernanostructures for ultrasensitive monitoring of morphine

Wei Chen[1,*], Lijun Yang[1], Chao Yan[1,4], Bangben Yao[1,2], Jianfeng Lu[1], Jianguo Xu[1,*], Guodong Liu[3,*]

[1]Engineering Research Center of Bioprocess, MOE, School of Food & Biological Engineering, Hefei University of Technology, Hefei, 230009, China
[2]Anhui Province Institute of Product Quality Supervision & Inspection, Hefei 230051, P. R. China
[3]Research Center for Biomedical and Health Science, School of Life and Health, Anhui Science & Technology University, Fengyang, 233100, China

*Correspondence should be addressed to. ORCID: 0000-0003-3763-1183 (W.C.) Email: chenweishnu@163.com, guodong.liu@ndsu.edu

Abstract

Overuse and abuse of morphine (MOP), one of the main components of pericarpium papaveris, have attracted increasing attention in the medical field owing to its pharmacological and toxicological activity. Herein, we proposed a new electrochemical nanobiosensor for MOP detection based on surface-confined building of Au@Pt-centered and multi-G-quadruplex/hemin wire-surrounded electroactive supernanostructures. The center Au@Pt was flower-shaped and irregular protruded, allowing substantial loading of multiple G-quadruplex wire/hemin complexes on its surface to accomplish the assembly of electroactive supernanostructures. Interestingly, as the supernanostructures were closely confined on the electrode surface, a significantly amplified electrochemical signal was thus obtained in the absence of MOP. Oppositely, the introduction of target MOP can induce an intense competitive effect and strongly destroy the assembly process, resulting in reduction of the electrochemical response that is corelated with the logarithmic concentration of MOP. Under optimal conditions, the electrochemical nanobiosensor is capable of highly sensitive detecting MOP at a dynamic concentration range from 1 ppt to 500 ppb. The limit of detection (LOD) is achieved as low as 0.69 ppt, and the practical application was confirmed by examining MOP from chafing dish condiments. We expect the electrochemical platform with the utilizing of this unique nanoarchitecture provides rational guidelines to design high performance analytical tools.

Keywords: food safety, morphine (MOP), Au@Pt, G-quadruplex, electroactive supernanostructures, signal amplification, electrochemical detection

Morphine (MP), a small molecule compound with molecular weight of 285.3 is a representative alkaloid that has both pharmacological and toxicological activity. Appropriate use of MOP injection in clinical can efficiently alleviate postoperative pains or carcinomatosis in patients.[1,2] However, MOP presents symptoms toxic when overused or abused, which can impose serious health issues, such as the disruption of central nervous system or even death.[3-5] Moreover, the long-term intake of MOP even at trace amounts can make people addictive, imposing strong mental tortures, severe physical damages, and unbearable economical burdens for addicts.[6-8] Accordingly, the MOP must be accurately monitored and maintained within safe ranges to prevent overdose or abuse induced toxication of MOP. Unfortunately, in order to enhance the flavor of the dishes, some catering staff illegally add pericarpium papaveris in the soup or condiment of the dishes. Long term contact of morphine in the dishes will also contributes to the addictive and harm of the health. Accurate identification of MOP components in various delicious dishes is of great importance.

Conventionally, the existing analytical techniques of colloidal gold immunochromatography,[9] chemiluminescence,[10,11] immune-assay,[12] high performance liquid chromatography (HPLC),[13,14] combined methods of GC-mass spectrometry (GC-MS)[15,16] and HPLC-mass spectrometry (HPLC-MS)[17] are frequently adopted for MOP analysis. Aside from their considerable achievements, the limited sensitivity of colloidal gold immunochromatography, chemiluminescence, and immune assay makes them non-suitable for the cases wherein ultrasensitive detection is required. Although the high sensitivity of HPLC, GC-MS, and HPLC-MS are benefited from their high

separation efficiencies, the needs of expensive and advanced instruments, professional technicians, as well as complicate operations can only partially solve the wide detection demands. Form this point, the development of alternative methods that can realize simple, cost-effective, and ultrasensitive detection of MOP are the ongoing goals.

Electrochemical biosensors are a type of valuable analytical tools for the detection of many analytes (e.g., proteins, metal ions, small molecules, cells, and viruses) due to their advantageous properties including high sensitivity, low cost, easy miniaturization, and operation simplicity.[18-22] Especially, advances in nanotechnology enable the application of nanomaterials, such as gold nanoparticles, silver nanoparticles, carbon nanoparticles, or some composite Au@Ag, Au@Pt to establish versatile electrochemical platforms.[23-26] Especially for Au@Pt liked materials, depend on their structural and electrochemical features, such as high surface area and loading capacity, inherent catalytic activity, and enhanced electron transfer ability, the nanomaterial-based electrochemical biosensors have been witnessed with remarkable progresses for sensitive and accurate detection of interested targets compared with the single component nanomaterials.[27-30] For instance, Zhou et al. has presented a hydroxyl pillar arene@AuNPs@g-C_3N_4 hybrid nanomaterial for ultrasensitive detection of prostate specific antigen.[31] Aliabadi et al. has used a modified carbon paste electrode for robust determination of MOP in urine sample.[32] Our group once reported the layer-by-layer assembly of dual AuNP-conjugates for ultrasensitive detection of ochratoxin (OTA).[33] Therefore, continuing exploration of electrochemical nanobiosensors is very promising to overcome the challenges faced by conventional methods for MOP detection.

Taken all into account, in this work, we proposed a new electrochemical nanobiosensor for accurate detection of MOP. The surface-confined building of Au@Pt-centered and multi-G-quadruplex/hemin wires-surrounded supernanostructures were fabricated on the sensing interface. Such supernanostructures combine the high loading capacity of Au@Pt with the strong electroactivity of G-quadruplex/hemin wire, which can not only be confined on the electrode surface via specific antibody-antigen recognition, but can also output remarkable electrochemical response that is inversely proportional to MOP concentration. The working principle, materials characterization, experimental condition optimization, assay performance investigation, and real sample analysis are detailly provided as follows, indicating the current study is promising to provide deep insights into the development of rational-designed nanoarchitectures for potential biochemical applications.

Experimental section

Reagents and chemicals

The chloroauric acid ($HAuCl_4$) and bovine serum albumin (BSA) were purchased from Sigma-Aldrich. The 11-decyl undecanoic acid (MUDA), MOP antibody (Ab-MOP), and MOP-BSA conjugate were provided by Shanghai Joey Biotechnology Company (Shanghai, China). The hemin was supplied by Aladdin reagent (Shanghai, China) and dissolved in DMSO to prepare a stock solution (50 mM). The TdT, dGTP, dATP, streptavidin (SAV), 4-(2-hydroxyethyl) piperazine-1 ethanesulfonic acid sodium salt (HEPES), and HPLC-purified oligonucleotides of elongation probe (EP) and Single G-

quadruplex probe (SGP) were purchased from Shanghai Sangon Biological Engineering Technology and Services Co. Ltd. (Shanghai, China). The sequences of EP and SGP are "5-Biotin-TTTTTTTTTTTT-3" and "5-Biotin-TTTTTTTTTTTTGGGTAGGGCGGGTTGGGT-3", respectively. All standard substances of MOP, cocaine (COC), methamphetamine (MET), clenbuterol (CL), salbutamol (SAL), and ractopamine (RAC) were sourced from the China Food and Drug Administration (Beijing, China). Unless otherwise specified, all other chemicals at analytical grade, such as $K_3Fe[CN]_6$ and $K_4Fe[CN]_6$, are provided by Sinopharm Chemical Reagent Company (Shanghai, China). The HEPES buffer (20 mM, pH 7.0) containing 5 mM KCl, 137 mM NaCl, and 0.75 mM Na_2HPO_4 was used to dilute the stock solution of hemin. The ultrapure water (Milli-A10 system, Millipore) with a resistivity of 18.2 MΩ/cm was used throughout the whole experiment.

Preparation of AuNPs

According to previously reported method, the AuNPs with an average diameter of 13 nm were prepared by reducing chloroauric acid with sodium citrate with minor modifications.[34] Briefly, 850 μL of chloroauric acid solution (5 g/L) was first added to 60 mL of double-distilled water and thoroughly mixed. The obtained mixture was then heated to 310 ℃ and pumped with 950 μL of 1 % trisodium citrate under a stirring condition. With the reaction proceeded, the color of the solution was gradually changed from colorless to purple, and finally to red. The resultant AuNPs were stabilized by stirring for another 5 min and stored after cooling down to room temperature. It should

be point out that all the glassware is required to be thoroughly cleaned with aqua regia solutions before usage.

Preparation of Au@Pt composite nanomaterials

To prepare the Au@Pt, 1 mL of 0.1 M ascorbic acid and 400 μL of 1% H_2PtCl_6 were immediately added into above synthesized AuNP solutions, from where we can see that the red-colored AuNPs was gradually turned to black. The obtained Au@Pt were stabilized by stirring for 10 min.

Preparation of Ab-MOP-Au@Pt-SAV

Prior to prepare the nanoconjugate of Ab-MOP-Au@Pt-SAV, the pH value of the Au@Pt solution was carefully adjusted to 8 using 0.1 M K_2CO_3. Afterwards, 2 μL of 1 mg/mL of Ab-MOP and 1 μL of 1 mg/mL of SAV were gently added into 500 μL of pretreated Au@Pt solution and incubated at room temperature for 1 h. Next, the blocking agent of 10 % BSA at a volume of 50 μL was added and stirred for 30 min to seal residual active sites for eliminating of non-specific adsorptions. Finally, the overused Ab-MOP and SAV were removed by centrifugation of the mixture at 7000 rpm for 8 min. The obtained precipitates were re-dissolved by 50 μL of 10% BSA and stored in 4 ℃ for subsequent use.

Preparation of G-quadruplex/hemin wires

The procedure for yielding of G-quadruplex wires was based on the reported TdT-promoted DNA polymerization with a slight modification.[35] In brief, a total volume of 10 μL reaction mixture containing 5 μL of 2 μM EP, 1.4 μL of dGTP, 0.6 μL of dATP, 0.5 μL of 20 U/μL TdT, and 2.5 μL of 5×TdT reaction buffer (1 M potassium cacodylate,

0.125M Tris, 0.05% Triton X-100, 5 mM $CoCl_2$, pH 7.2) was kept at 37 ℃ for 1 h to implement the catalytic reaction. The obtained solution was then terminated at 95 ℃ for 3 min and successively incubated with 5μL of 200 mM K^+ and 5 μL of 0.2 mM hemin to form the complex of G-quadruplex/hemin wire. The diagram for the preparation and of G-quadruplex/hemin wires and its characterization can be seen in **Figure S1**.

Construction of electrochemical nanobiosensor

Before fabrication of the electrochemical nanobiosensor, the gold electrode (diameter 3 mm) was polished on a flat pad by 0.05 μm α-Al_2O_3 slurry to obtain a mirror-like surface, followed by immersed into a fresh-prepared piranha solution (H_2SO_4/H_2O_2, volume ratio 3:1) for 30 min. Then, the electrode was ultrasonically cleaned in ethanol and water for 5 min, and electrochemically cleaned in a 0.5 M H_2SO_4 solution by potential scanning from −0.2 to 1.5 V until a stable reproducible voltammetric peak was obtained. After washing with ultrapure water and drying by a nitrogen stream, the pretreated gold electrode was added with 30 μL of 0.5 mM MUDA and incubated at room temperature for 3 h. For activation of MUDA, the electrode was then immersed into 30 μL of the EDC/NHS solution (75mM EDC and15mM NHS) and reacted in darkness at room temperature for 1 h. This was followed by addition of 10% BSA (30 μL) to block the remaining sites at 37 ℃ for 1 h and treated with Ab-MOP-Au@Pt-SAV (30 μL) with a certain concentration of MOP at 37 ℃ for 40 min. At last, 5 μL of G-quadruplex/hemin wires was dropped to form the supernanostructures at 37 ℃ for 30 min. Notable, the rinsing by double-distilled water and drying by nitrogen stream

were needed to be performed after accomplish each of the assembly step.

Electrochemical measurements

The electrochemical assays of cyclic voltammetry (CV), electrochemical impedance spectroscopy (EIS), and differential pulse voltammetry (DPV) were commonly performed on a CHI 660D electrochemical workstation (Chenhua Instrument Company of Shanghai, China) at room temperature. A conventional three-electrode system consisting of an assembled electrode as the working electrode, a platinum wire as the auxiliary electrode, and an Ag/AgCl as the reference electrode was employed to construct the electrolysis cell. For CV scanning, it was performed in 5 mM $[Fe(CN)_6]^{3-/4-}$ (containing 0.1 M KCl) with a scanning potential from -0.2 to 0.6 V and a scanning rate of 50 mV/s. For EIS measurement, it was also analyzed in 5 mM $[Fe(CN)_6]^{3-/4-}$ (containing 0.1 M KCl). The frequency range was set from 10 kHz to 0.1 Hz. For DPV detection, it was recorded in 20 mM HEPES solution (50 mM KCl, 200 mM NaCl, pH 8.0), which was thoroughly degassed under the stream of nitrogen for 30 min before usage. The parameters of pulse amplitude and pulse period were of 50 mV and 50 ms, respectively.

Results and discussion

Principle of the electrochemical biosensor

To construct the electrochemical nanobiosensor, the classic competitive assay was adopted for the small molecule of MOP. As illustrated in **Scheme 1**, the MUDA was initially immobilized on the gold electrode via the formation of an Au-S bond and then

covalently conjugated with the MOP-BSA via a classical covalent reaction. The remaining sites is totally blocked by BSA. In the absence of target MOP, the prepared Anti-MOP-Au@Pt-SAV can directly recognize the immobilized MOP-BSA, thereby leading to the substantial accumulation of the G-quadruplex/hemin wires through the specific streptavidin-biotin interaction. In this case, the Au@Pt-centered and muti-G-quadruplex/hemin wires surrounded supernanostructures enriched with a mass of electroactive molecules of hemin are assembled. Specially, owing to the confinement of such electroactive supernanostructures at the electrode surface and the outstanding electron transfer ability of Au@Pt, a remarkable electronical response from the redox reaction of hemin can be obtained. Notably, the G-riched wires for the formation of G-quadruplex/hemin wires are produced and also characterized in **Figure S1** by a typical TdT-mediated polymerization with the presence of dGTP and dATP at a ratio of 7:3, which can be tightly integrated with hemin to experience a configuration change to from G-quadruplex/hemin wires with the help of potassium ion. However, upon addition of target MOP into the system, it can occupy a part of the recognition sites on Anti-MOP-Au@Pt-SAV, resulting in the concentration reduction of the free Anti-MOP-Au@Pt-SAV to be captured on the electrode surface. Therefore, the assembled electroactive supernanostructures are correspondingly decreased with a weakened electronical response. If the MOP was sufficiently presented, the strong competitive effect cannot build any supernanostructures on the surface, and no detectable signals can be reported. Along this line, a "signal-off" electronical biosensor based on the surface-confined building of Au@Pt-centered and multi-G-quadruplex/hemin wires-

surrounded electroactive supernanostructures for ultrasensitive determination of MOP has been achieved.

Preferred position for Scheme 1

Materials characterization

The morphology of AuNPs, Au@Pt, and Ab-MOP-Au@Pt-SAV nanoconjugates were all characterized by transmission electron microscopy (TEM) and dynamic light scattering (DLS). As displayed in **Figure 1A**, the AuNPs exhibited a typical spherical shape and were uniformly distributed with an average diameter about 13 nm. After coated with Pt, the obtained Au@Pt bimetallic ally (**Figure 1B**) shown a spherical flower structures but with a rough surface. The average diameter is increased to 18 nm. Subsequently, the further absorption of Ab-MOP and SAV onto the Au@Pt resulted in the obtained Ab-MOP-Au@Pt-SAV (**Figure 1C**) with a slightly smoothed surface and an enlarged average diameter of 21 nm. The distinct morphologies changes and obvious difference in diameters among **Figure 1A, Figure 1B,** and **Figure 1C** strongly suggests the successful synthesis of AuNPs, Au@Pt, and Ab-MOP-Au@Pt-SAV nanoconjugates.

Preferred position for Figure 1

Electrochemical characterization of the assembly procedure

The layer-by-layer interfacial fabrication processes were characterized by the representative techniques of cyclic voltammogram (CV) and electrochemical impedance spectra (EIS) in 5 mM $[Fe(CN)_6]^{3-/4-}$ (containing 0.1 M KCl). As shown in

Figure 2A, the voltammograms had a couple of well-defined reversible redox peak of $[Fe(CN)_6]^{3-/4-}$ at the bare Au surface (curve a). After modified with MUDA and activated by EDC/NHS, the electron transfer was inhibited with a slower rate taking account of its weak conductivity compared with gold (curve b). The following introduction of MOP-BSA (curve c) to establish specific binding sites and addition of BSA (curve d) to cover the non-specific binding sites prevented further the electron transfers in terms of their poor electroconductivities and stereo-hindrance effects. Likewise, a distinctive and continuous decline of the redox peak currents were obtained when sequentially modify the BSA-blocked gold electrode with Ab-MOP-Au@Pt-SAV nanocomposites (curve e) and G-quadruplex/hemin wires (curve f). The reasonable results are primarily attributed to proteins on Ab-MOP-Au@Pt-SAV and negative-charged phosphate backbones on G-quadruplex/hemin wires provide strong electrostatic repulsion forces to hinder the electron transfer of the working electrode.

Figure 2B depicts Nyquist plots of the EIS. The semicircle diameter is equal to the electron transfer resistance (R_{et}) at higher frequency, while the straight line is related to the diffusion process at low frequency. One can find that the EIS of the bare gold electrode was almost straight (curve a), implying the diffusion of $[Fe(CN)_6]^{3-/4-}$. Compared with the gold electrode, the R_{et} value increased (curve b, c, d, e, and f) in sequence due to the augment of interfacial negative charge and stereo-hindrance effect causing an increased barrier for the ferricyanide diffused to the biosensing interface. The observations in **Figure 2A** and **Figure 2B** are consistent well with each other, convincing the electrochemical nanobiosensor has been fabricated to be appropriate for

electrochemical analysis.

Preferred position for Figure 2

Feasibility investigation

To examine the feasibility for MOP biosensing, the DPV measurements were performed before and after exposed to MOP at the concentration of 1 ppm. As collected in **Figure 3**, we can see that the presence of target MOP at a trace amount can lead to a significant decrease (curve d vs c) of the peak current that is closed to the base line. The net signal decrease ($\triangle I=I_0-I$) deduced by the electrochemical response in the absence (I_0) and presence (I) of target MOP is as large as about 157.77 nA, indicating the already built nanosensing strategy is available for MOP analysis. Besides, in order to validate if the assembled nanostructure can positively promote signal amplification, a control MOP detection platform based on the employment of a biotin-labeled SGP moiety to form common nanostructures as the reporter has been assembled to identically detect target MOP. The diagram of the control method is schematically provided in **Scheme S1**. Comparatively, although the introduction of MOP can also decrease the current of the control platform (curve b vs a), the corresponding signal decrease is only about 57.33 nA, which is much less than the current of proposed sensing method. As a consequence, we can surely confirm that the unique supernanostructures assembly method shows a sensitive response that can benefit robust MOP detection.

Preferred position for Figure 3

Quantitative analysis of MOP

To investigate the assay performance, the sensitivity and dynamic range were evaluated by DPV measurements under optimized experimental conditions (**Figure S2**). As shown in **Figure 4A**, the peak current decreased with the increase of MOP concentration from 1 ppt to 1 ppm, indicating that the assembled supernanostructure is inversely proportional to the concentration of MOP. **Figure 4B** shows a linear plot of the peak current versus logarithm of the MOP concentration. The corresponding regression equation was fitted as $I = -16.39 \text{ Log } C_{mop}+84.21$ with a correlation coefficient of 0.9848, where I and log C_{mop} represent the peak current and logarithm of the MOP concentration, respectively. The linear response is from 1 ppt to 500 ppb, which is over a dynamic range of 5 orders of magnitude. Of note, this extraordinary sensing range can be attributed to both the Au@Pt and multi-G-quadruplex/hemin wire assisted surface confined electroactive supernanostructures. Hereinto, the background signal can be dramatically enlarged for wide range sensing. The detection limit is estimated to be 0.69 ppt based on 3σ/slope (σ, standard deviation of the blank sample). Compared with previously reported method such as HPLC, GC-MS, lateral flow strip, molecularly imprinted polymer-modified electrode, and quantum dots based immunoassays,[9,36-40] the sensitivity is obviously improved for small molecules detection. Detailed comparison is provided in **Table S1**. These results indicate that the building of electroactive supernanostructures on electrode surface can sensitively reveal the change of MOP concentration, which can be attributed to the factors of high surface area, loading capacity, and electron transfer ability of Au@Pt, as well as the

substantial enrichment of hemin in this supernanostructures.

Preferred position for Figure 4

Specificity study

Except for the sensitivity, specificity is another important element to evaluate the successful construction of electrochemical sensing platform. To assess the specificity, the target MOP was tested against other randomly selected and common small molecules of cocaine (COC), methamphetamine (MET), clenbuterol (CL), salbutamol (SAL), and ractopamine (RAC) at the same concentration. As expected in **Figure 5**, no signal decrease in the peak current was observed upon addition of COC, MET, CL, SAL, and RAC, while the introduction of target MOP made a sharp decrease of the peak current that was extremely lower than the non-target analytes. This comparison confirms the detection system is offered with an excellent specificity, which is ascribed mainly to the accurate antibody-antigen recognition to obstruct the supernanostructures assembly for MOP, but permit the normal supernanostructures assembly for other non-target analytes.

Preferred position for Figure 5

Real sample analysis

As MOP is frequently illegal added in food to enhance its flavor, its abuse has brought serious food safety risks to consumers.[37] To verify the practical application ability for detecting of MOP added food samples, the mimic food samples were prepared by

spiking MOP into chafing dish condiments, which was pre-treated by dissolving and filtration according to our reported method.[9] As displayed in **Table 1**, the doped MOPs at indicated final concentrations of 1 ppt, 5 ppb, and 500 ppb were measured with good recoveries from 94.8 % to 102.7%. The obtained RSD values were all below 5%. Given that the spiked MOP is representatively selected at low (1 ppt), medium (5 ppb), and high (500 ppb) concentrations, these results powerfully reveal that our proposed system has great potential for quantitative determination of MOP in real food samples.

Preferred position for Table 1

Conclusion

In conclusion, we have developed an electrochemical nanobiosensor for MOP analysis on the basis of the confinement and removal of electroactive supernanostructures. Structurally, the electroactive supernanostructure is Au@Pt centered and multi-G-quadruplex/hemin wires-surrounded. The presence of MOP can trigger an obvious electrochemical signal change. In comparison with previous reported results, the electrochemical nanobiosensor is demonstrated with a lower LOD of 0.69 ppt, as well as a wider linear range from 1 ppt to 500 ppb for MOP detection. As evidence of its potential practical application, the contents of MOP in chafing dish condiments were successfully determined. Therefore, the method with wide linear range and high sensitivity and specificity is highly expected to be an excellent choice for daily detection of various target analytes in trace levels.

ASSOCIATED CONTENT

Supporting Information

The Supporting Information is available free of charge. Contents of schematic description of the traditional assembly of nanostructures for detection, the electrophoresis characterization results of TdT-based extension of long DNA wires, detailed optimization results of the detection conditions and also comparisons result with other reported methods.

AUTHOR INFORMATION

Corresponding Author

Wei Chen- Engineering Research Center of Bioprocess, MOE, School of Food & Biological Engineering, Hefei University of Technology, Hefei, 230009, China; orcid.org/0000-0003-3763-1183; Email: chenweishnu@163.com

Jianguo Xu- Engineering Research Center of Bioprocess, MOE, School of Food & Biological Engineering, Hefei University of Technology, Hefei, 230009, China; orcid.org/ 0000-0002-0187-2623; Email: jgxu0816@163.com

Guodong Liu- Research Center for Biomedical and Health Science, School of Life and Health, Anhui Science & Technology University, Fengyang, 233100, China; guodong.liu@ndsu.edu

Authors

Lijun Yang- Engineering Research Center of Bioprocess, MOE, School of Food & Biological Engineering, Hefei University of Technology, Hefei, 230009, China

Chao Yan- Engineering Research Center of Bioprocess, MOE, School of Food & Biological Engineering, Hefei University of Technology, Hefei, 230009, China

Bangben Yao- Anhui Province Institute of Product Quality Supervision & Inspection, Hefei 230051, P. R. China

Jianfeng Lu- Engineering Research Center of Bioprocess, MOE, School of Food & Biological Engineering, Hefei University of Technology, Hefei, 230009, China

Notes

The authors declare no competing financial interest.

Acknowledgments

This work was financially supported by the grants of the Ministry of Science and Technology of China (Grants No. 2018YFC1603606, 2017YFF0208600), the National Natural Science Foundation China (Grants No. 21475030, 21804028), the Anhui Provincial Natural Science Foundation (Grant No. 1908085QC121), the Fundamental Research Fund for central university (Grants No. 2017HGPA0162, JZ2019HGTB0068, PA2017GDQT0018), the Fund of State Key Laboratory of Chemo/Biosensing and Chemometrics (Hunan University), and China Agriculture Research System-48 (CARS-48).

References

(1) Gilron, I.; Bailey, J. M.; Tu, D.; Holden, R. R.; Weaver, D. F.; Houlden, R. L. Morphine, Gabapentin, or Their Combination for Neuropathic Pain. *The New England Journal of Medicine* 2005, 352, 1324-1334.

(2) Anand, K. J. S.; Hickey, P. R. Halothane-morphine compared with high-dose sufentanil for anesthesia and postoperative analgesia in neonatal cardiac surgery. *The New England Journal of Medicine* 1992, 326, 1-9.

(3) Mohamed, M. A.; El-Gendy, D. M.; Ahmed, N.; Banks, C. E.; Allam, N. K. 3D spongy graphene-modified screen-printed sensors for the voltammetric determination of the narcotic drug codeine. *Biosens. Bioelectron.* 2018, 101, 90-95.

(4) Lloret-Linares, C.; Miyauchi, E.; Luo, H.; Labat, L.; Bouillot, J. L.; Poitou, C.; Oppert, J. M.; Laplanche, J. L.; Mouly, S.; Scherrmann, J. M.; Uchida, Y.; Tachikawa, M.; Terasaki, T.; Bergmann, J. F.; et al. Oral Morphine Pharmacokinetic in Obesity: The Role of P-Glycoprotein, MRP2, MRP3, UGT2B7, and CYP3A4 Jejunal Contents and Obesity-Associated Biomarkers. *Mol. Pharmaceut.* 2016, 13, 766-773.

(5) Del Bello, F.; Diamanti, E.; Giannella, M.; Mammoli, V.; Marchioro, C.; Mattioli, L.; Titomanlio, F.; Piergentili, A.; Quaglia, W.; Benedetti, G.; Varrone, M.; Pigini, M. Low Doses of Allyphenyline and Cyclomethyline, Effective against Morphine Dependence, Elicit an Antidepressant-like Effect. *ACS. Med. Chem. Lett* 2012, 3, 535-539.

(6) Devereaux, A. L.; Mercer, S. L.; Cunningham, C. W. DARK Classics in Chemical Neuroscience: Morphine. *ACS. Chem. Neurosci* 2018, 9, 2395-2407.

(7) López, P.; Pereboom-de Fauw, D. P. K. H.; Mulder, P. P. J.; Spanjer, M.; de Stoppelaar, J.; Mol, H. G. J. Straightforward analytical method to determine opium alkaloids in poppy seeds and bakery products. *Food. Chem* 2018, 242, 443-450.

(8) Navaee, A.; Salimi, A.; Teymourian, H. Graphene nanosheets modified glassy carbon electrode for simultaneous detection of heroine, morphine and noscapine. *Biosens. Bioelectron* 2012, 31, 205-211.

(9) Chen, W.; Li, X. N.; Wu, Q.; Yao, L.; Xu, J. Rapid and easy determination of morphine in chafing dish condiments with colloidal gold labeling based lateral flow strips. *Food. Sci. Hum. Well*. 2019, 8, 40-45.

(10) Terry, J. M.; Smith, Z. M.; Learey, J. J.; Shalliker, R. A.; Barnett, N. W.; Francis, P. S. Chemiluminescence detection of heroin in illicit drug samples. *Talanta.* 2013, 116, 619-625.

(11) Shahvar, A.; Saraji, M.; Shamsaei, D. Smartphone-based chemiluminescence sensing for TLC imaging. *Sensor. Actuat. B-Chem.* 2018, 255, 891-894.

(12) Gandhi, S.; Suman, P.; Kumar, A.; Sharma, P.; Capalash, N.; Suri, C. R. Recent

advances in immunosensor for narcotic drug detection. *Bioimpacts.* 2015, 5, 207-213.

(13) Hartley, R.; Green, M.; Quinn, M.; Levene, M. I. Analysis of morphine and its 3- and 6-glucuronides by high performance liquid chromatography with fluorimetric detection following solid phase extraction from neonatal plasma. *Biomed. Chromatogr.* 2010, 7, 34-37.

(14) Jafari-Nodoushan, M.; Barzin, J.; Mobedi, H. A stability-indicating HPLC method for simultaneous determination of morphine and naltrexone. *J. Chromatogr. B.* 2016, 1011, 163-170.

(15) Meatherall, R., GC-MS Quantitation of Codeine, Morphine, 6-Acetylmorphine, Hydrocodone, Hydromorphone, Oxycodone, and Oxymorphone in Blood. *J. Anal. Toxicol.* 2005, 29, 301-308.

(16) Meadway, C.; George, S.; Braithwaite, R. A rapid GC–MS method for the determination of dihydrocodeine, codeine, norcodeine, morphine, normorphine and 6-MAM in urine. *Forensic. Sci. Int.* 2002, 127, 136-141.

(17) Zheng, M.; Mcerlane, K. M.; Ong, M. C. High-performance liquid chromatography-mass spectrometry-mass spectrometry analysis of morphine and morphine metabolites and its application to a pharmacokinetic study in male Sprague-Dawley rats 1. *J. Pharmaceut. Biomed.* 1998, 16, 971-980.

(18) Sheng, M.; Gao, Y.; Sun, J.; Gao, F. Carbon nanodots-chitosan composite film: A platform for protein immobilization, direct electrochemistry and bioelectrocatalysis. *Biosens. Bioelectron.* 2014, 58, 351-358.

(19) Gao, F.; Gao, C.; He, S.; Wang, Q.; Wu, A. Label-free electrochemical lead (II)

aptasensor using thionine as the signaling molecule and graphene as signal-enhancing platform. *Biosens. Bioelectron.* 2016, 81, 15-22.

(20) Xia, S.; Zhu, P.; Pi, F.; Zhang, Y.; Li, Y.; Wang, J.; Sun, X. Development of a simple and convenient cell-based electrochemical biosensor for evaluating the individual and combined toxicity of DON, ZEN, and AFB1. *Biosens. Bioelectron.* 2017, 97, 345-351.

(21) Mahato, K.; Kumar, A.; Maurya, P. K.; Chandra, P. Shifting paradigm of cancer diagnoses in clinically relevant samples based on miniaturized electrochemical nanobiosensors and microfluidic devices. *Biosens. Bioelectron.* 2018, 100, 411-428.

(22) Faria, H. A. M.; Zucolotto, V. Label-free electrochemical DNA biosensor for zika virus identification. *Biosens. Bioelectron.* 2019, 131, 149-155.

(23) Zhao, L.; Blackburn, J.; Brosseau, C. L. Quantitative Detection of Uric Acid by Electrochemical-Surface Enhanced Raman Spectroscopy Using a Multilayered Au/Ag Substrate. *Anal. Chem*. 2015, 87, 441-447.

(24) Kaito, T.; Mitsumoto, H.; Sugawara, S.; Shinohara, K.; Uehara, H.; Ariga, H.; Takakusagi, S.; Hatakeyama, Y.; Nishikawa, K.; Asakura, K. K-Edge X-ray Absorption Fine Structure Analysis of Pt/Au Core–Shell Electrocatalyst: Evidence for Short Pt-Pt Distance. *Indian. J. Chem. A.* 2014, 118, 8481-8490.

(25) Lapp, A. S.; Duan, Z.; Marcella, N.; Luo, L.; Genc, A.; Ringnalda, J.; Frenkel, A. I.; Henkelman, G.; Crooks, R. M. Experimental and Theoretical Structural Investigation of AuPt Nanoparticles Synthesized Using a Direct Electrochemical Method. *J. Am. Chem. Soc.* 2018, 140, 6249-6259.

(26) Hong, W.; Li, C. W. Microstructural Evolution of Au@Pt Core–Shell Nanoparticles under Electrochemical Polarization. *ACS. Appl. Mater. Inter.* 2019, 11, 30977-30986.

(27) Li, H.; Chen, Q.; Mehedi, H. M.; Chen, X.; Ouyang, Q.; Guo, Z.; Zhao, J. A magnetite/PMAA nanospheres-targeting SERS aptasensor for tetracycline sensing using mercapto molecules embedded core/shell nanoparticles for signal amplification. *Biosens. Bioelectron.* 2017, 92, 192-199.

(28) Xia, X.; Wang, Y.; Yang, H.; Dong, Y.; Zhang, K.; Lu, Y.; Deng, R.; He, Q. Enzyme-free amplified and ultrafast detection of aflatoxin B1 using dual-terminal proximity aptamer probes. *Food. Chem.* 2019, 283, 32-38.

(29) Zhou, M.; Wang, D.; Mirkin, M. V. Electrochemical Evaluation of the Number of Au Atoms in Polymeric Gold Thiolates by Single Particle Collisions. *Anal. Chem.* 2018, 90, 8285-8289.

(30) Kato, D.; Kamata, T.; Kato, D.; Yanagisawa, H.; Niwa, O. Au Nanoparticle-Embedded Carbon Films for Electrochemical As^{3+} Detection with High Sensitivity and Stability. *Anal. Chem*. 2016, 88, 2944-2951.

(31) Zhou, X.; Yang, L.; Tan, X.; Zhao, G.; Xie, X.; Du, G. A robust electrochemical immunosensor based on hydroxyl pillar arene@AuNPs@g-C3N4 hybrid nanomaterial for ultrasensitive detection of prostate specific antigen. *Biosens. Bioelectron.* 2018, 112.

(32) Aliabadi, A.; Rounaghi, G. H. A novel electrochemical sensor for determination of morphine in a sub-microliter of human urine sample. *Electroanal. Chem.* 2019, 832, 204-208.

(33) Chen, W.; Yan, C.; Cheng, L.; Yao, L.; Xue, F.; Xu, J. An ultrasensitive signal-on electrochemical aptasensor for ochratoxin A determination based on DNA controlled layer-by-layer assembly of dual gold nanoparticle conjugates. *Biosens. Bioelectron.* 2018, 117, 845-851.

(34) Li, L.; Li, B.; Cheng, D.; Mao, L. Visual detection of melamine in raw milk using gold nanoparticles as colorimetric probe. *Food. Chem.* 2010, 122, 895-900.

(35) Xu, J.; Yan, C.; Wang, X.; Yao, B.; Lu, J.; Liu, G.; Chen, W. Ingenious Design of DNA Concatamers and G-Quadruplex Wires Assisted Assembly of Multibranched DNA Nanoarchitectures for Ultrasensitive Biosensing of miRNA. *Anal. Chem.* 2019, 91, 9747-9753.

(36) Yeh, W. M.; Ho, K. C. Amperometric morphine sensing using a molecularly imprinted polymer-modified electrode. *Anal. Chim. Acta.* 2005, 542, 76-82.

(37) Zhang, C.; Han, Y.; Lin, L.; Deng, N.; Chen, B.; Liu, Y. Development of Quantum Dots-Labeled Antibody Fluorescence Immunoassays for the Detection of Morphine. *J. Agr. Food. Chem.* 2017, 65, 1290-1295.

(38) Abdolmohammad-Zadeh, H.; Zamani, A.; Shamsi, Z. Preconcentration of morphine and codeine using a magnetite/reduced graphene oxide/silver nano-composite and their determination by high-performance liquid chromatography. *J. Chromatogr. A.* 2019, 1590, 2-9.

(39) Cone, E. J.; Welch, P.; Mitchell, J. M.; Paul, B. D. Forensic Drug Testing for Opiates: I. Detection of 6-Acetylmorphine in Urine as an Indicator of Recent Heroin Exposure; Drug and Assay Considerations and Detection Times. *J. Anal. Toxicol.* 1991,

15, 1-7.

(40) Costin, J. W.; Lewis, S. W.; Purcell, S. D.; Waddell, L. R.; Francis, P. S.; Barnett, N. W. Rapid determination of Papaver somniferum alkaloids in process streams using monolithic column high-performance liquid chromatography with chemiluminescence detection. *Anal. Chim. Acta.* 2007, 597, 19-23.

Captions of Figures

Scheme 1. Schematic illustration of the electrochemical biosensor based on surface-confined building of Au@Pt-centered and multi-G-quadruplex/hemin wires-surrounded electroactive supernanostructures for "signal-off" electrochemical determination of MOP.

Figure 1. Typical images of TEM and DLS corresponding to AuNPs (A), Au@Pt (B), and Ab-MOP-Au@Pt-SAV(C), respectively. The obvious changes of their morphologies and diameters indicates the synthesis of AuNPs, Au@Pt, and Ab-MOP-Au@Pt-SAV.

Figure 2. (A) CV and (B) EIS signals of the bare Au electrode at different modification stages: (a) bare Au; (b) Au/Activated MUDA; (c) Au/Activated MUDA/MOP-BSA; (d) Au/Activated MUDA/MOP-BSA/BSA; (e) Au/Activated MUDA/MOP-BSA/BSA/Ab-MOP-Au@Pt-SAV; (f) Au/Activated MUDA/MOP-BSA/BSA/Ab-MOP-Au@Pt-SAV/G-quadruplex-hemin wires.

Figure 3. Comparison of the supernanostructures based electrochemical nanobiosensor (curve d vs c) with common nanostructures based electrochemical nanobiosensor (curve b vs a) in the absence and presence of same target MOP concentration (1 ppm), respectively.

Figure 4. (A) DPV measurements of the electrochemical nanobiosensor in the presence of a variety of MOP concentrations (From top to bottom: 0, 1ppt, 10 ppt, 100 ppt, 1 ppb, 10 ppb, 50 ppb, 100 ppb, 500 ppb, and 1ppm). (B) The Plotted calibration curve of the peak current as a function of the logarithm of the target MOP concentration. Inset provides the estimated regression equation. Error bars are obtained from three parallel tests.

Figure 5. Collected peak currents by histogram to show different electrochemical responses of MOP, COC, MET, CL, SAL, and RAC, respectively. Error bars are obtained from three parallel tests.

Table 1. Recoveries of MOP from chafing dish condiments (N=5)

Scheme 1

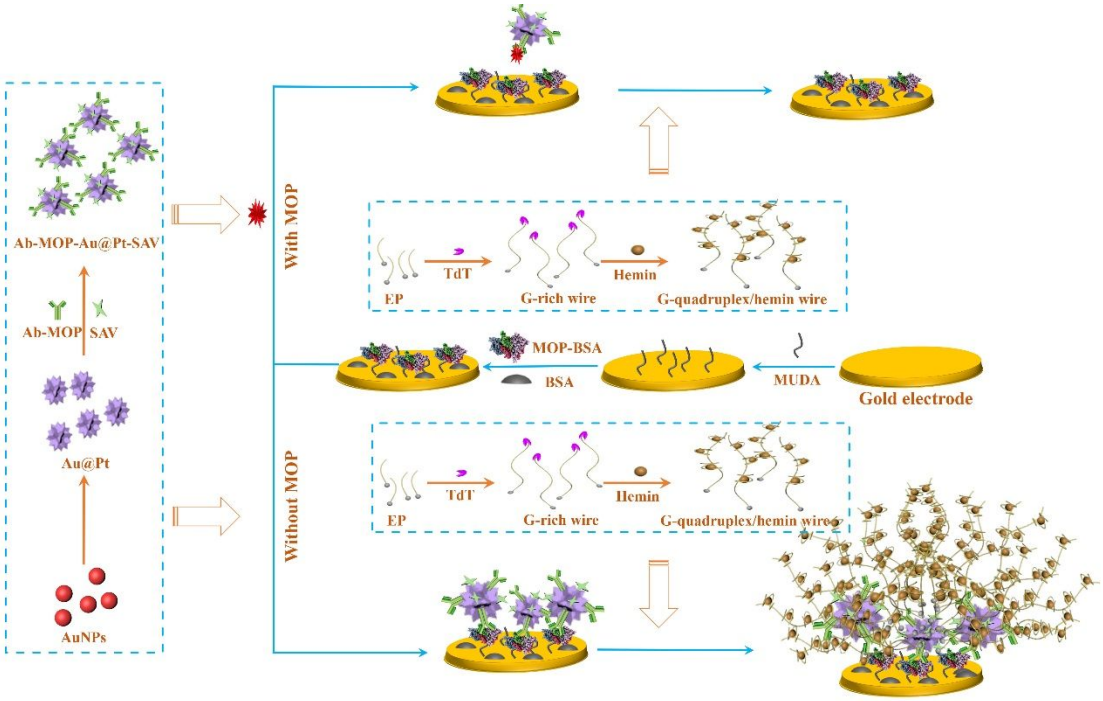

Scheme 1

Figure 1

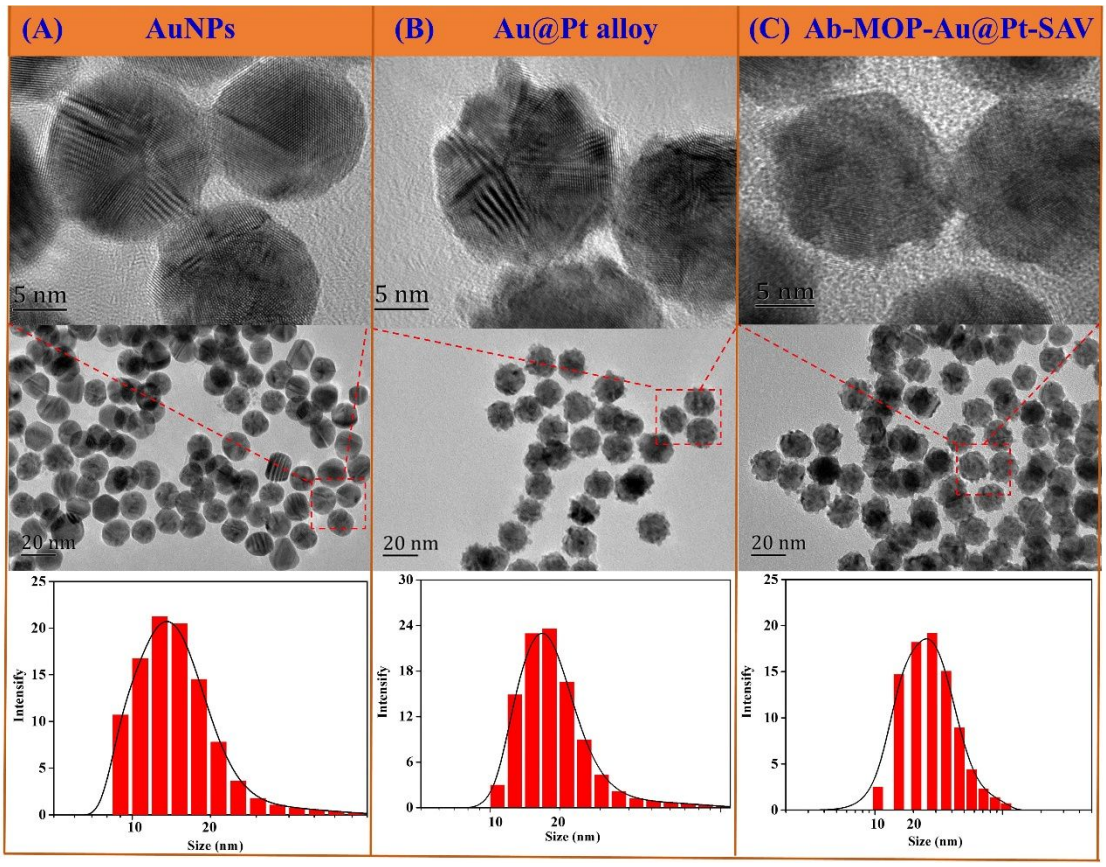

Figure 1

546

547 **Figure 2**

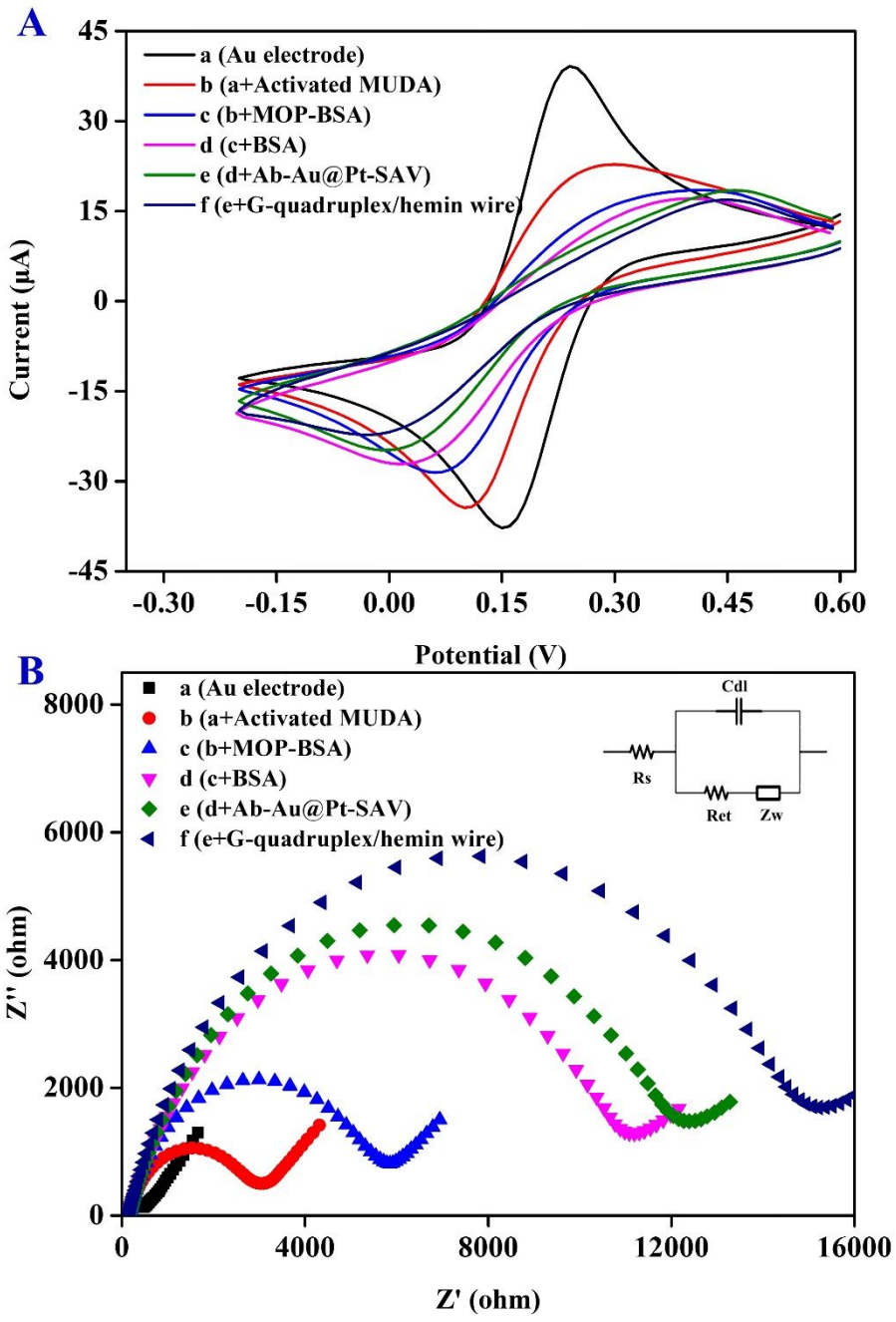

548

549 **Figure 2**

550

551

552

553

554 **Figure 3**

555

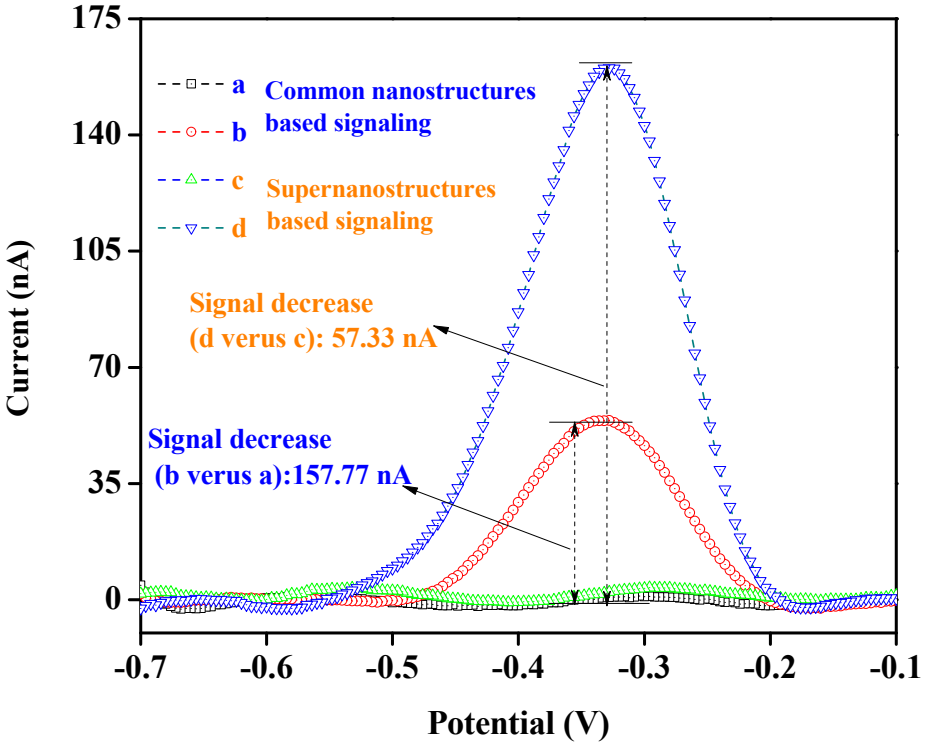

556

557 **Figure 3**

558

559 **Figure 4**

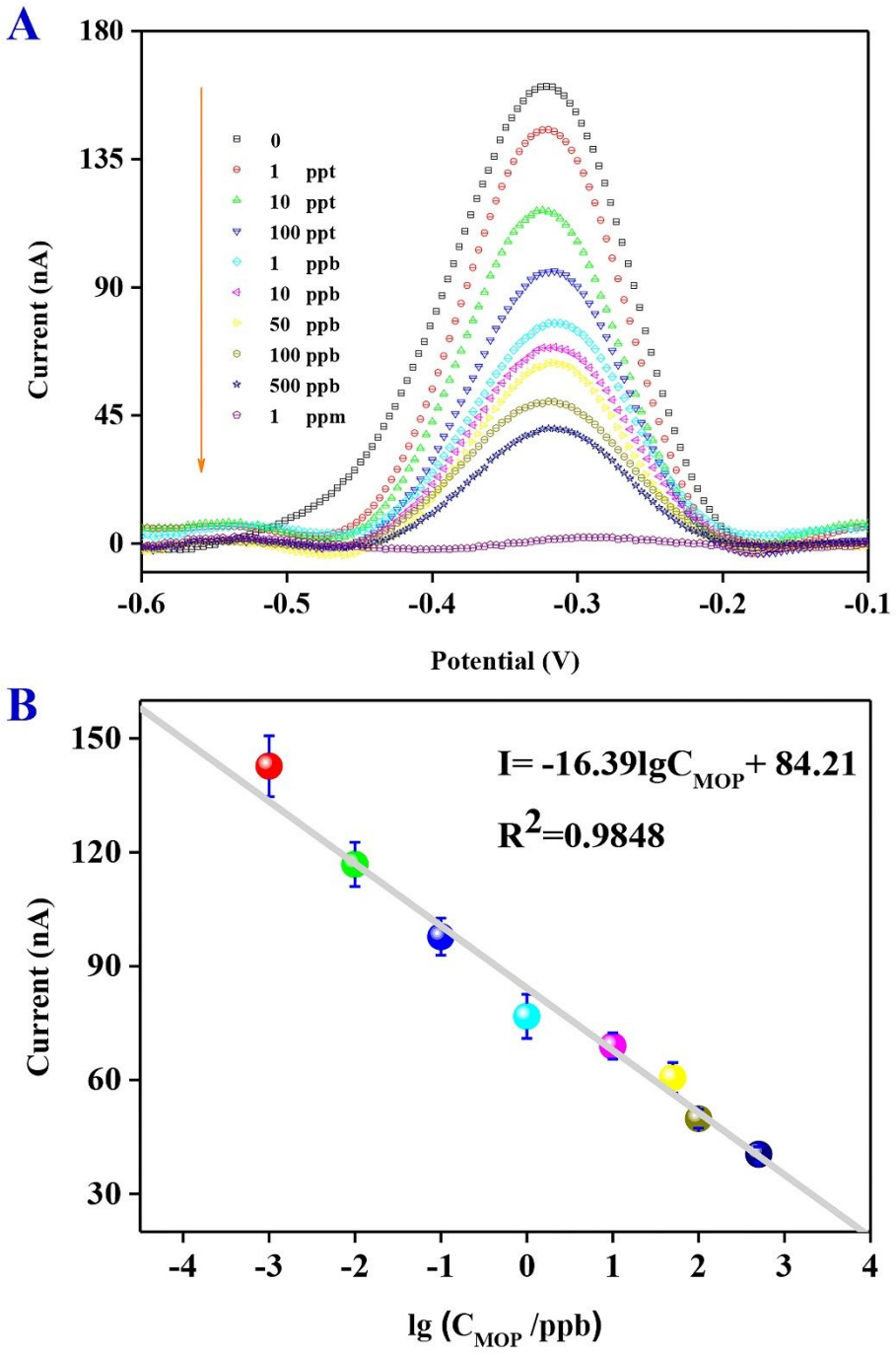

560

561 **Figure 4**

562

563 **Figure 5**

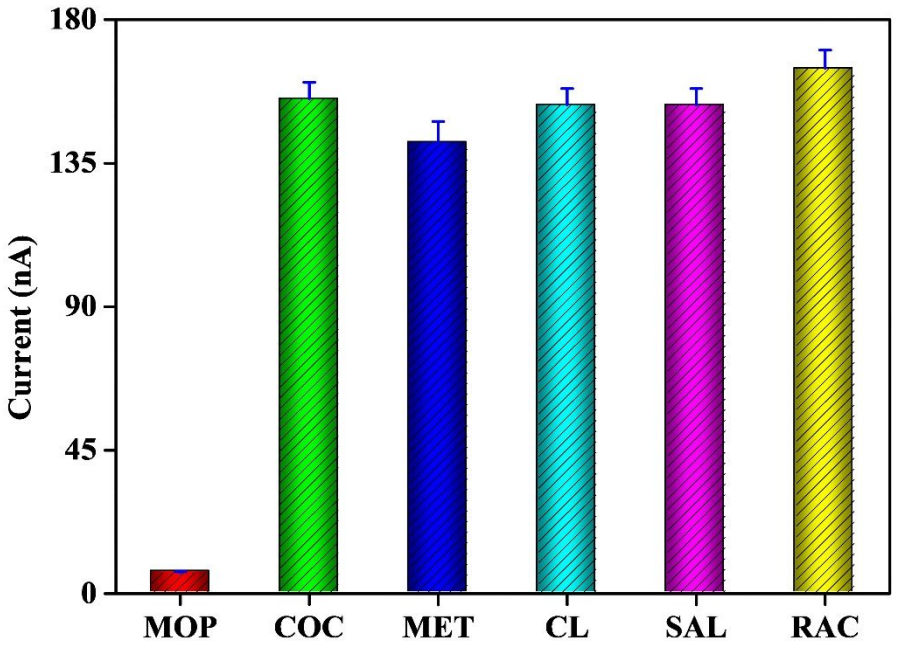

564

565 **Figure 5**

566

567

Table 1

Sample	Added (ppb)	Found (ppb)	Recovery (%)	RSD (%)
1	0.001	0.00096	96.0	3.1
2	5	4.74	94.8	4.2
3	500	513.5	102.7	2.7

TOC Graphic

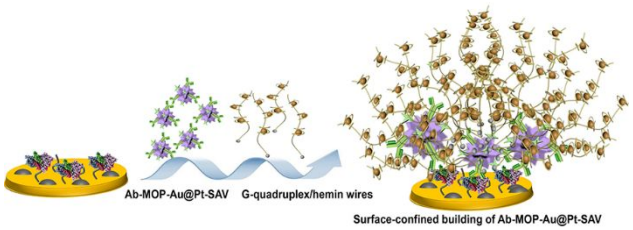
Ab-MOP-Au@Pt-SAV
G-quadruplex/hemin wires
Surface-confined building of Ab-MOP-Au@Pt-SAV